Excitation based cone-beam X-ray luminescence tomography of nanophosphors with different concentrations

Peng Gao*, Huangsheng Pu*, Junyan Rong, Wenli Zhang, Tianshuai Liu, Wenlei Liu, and Hongbing Lu§
Department of Biomedical Engineering, Fourth Military Medical University, Xi'an, Shaanxi 710032, China
§*luhb@fmmu.edu.cn*

***Abstract*—Cone-beam X-ray luminescence computed tomography (CB-XLCT), which has been proposed as a new molecular imaging modality recently, can obtain both anatomical and functional tomographic images of an object efficiently, with the excitation of nanophosphors *in vivo* or *in vitro* by cone-beam X-rays. However, the ill-posedness of the CB-XLCT inverse problem degrades the image quality and makes it difficult to resolve adjacent luminescence targets with different concentrations, which is essential in drug delivery and treatment monitoring *in vivo*. To address this problem, a multi-voltage excitation imaging scheme combined with principal component analysis is proposed in this study. Imaging experiments performed on physical phantoms by a custom-made CB-XLCT system demonstrate that two adjacent targets, with the concentration differences of 50 and 100 mg/ml and an edge-to-edge distance of 0 mm, can be effectively resolved.**

Keywords—image reconstruction techniques; optical tomography;X-ray imaging; principal component analysis

I. INTRODUCTION

X-ray luminescence computed tomography (XLCT) has been proposed as a promising hybrid molecular imaging modality in recent years with the development of X-ray excitable nanophosphors [1-5]. When irradiated by X-rays, nanophosphors in the imaging object emit visible or near-infrared (NIR) light that can be detected by an optical detector. Base on the imaging and reconstruction model, the distribution and concentration of the nanophosphors inside imaging object can be recovered. Compared with other optical molecular imaging such as bioluminescence tomography (BLT) [6, 7] and fluorescence molecular tomography (FMT) [8, 9], XLCT has several advantages with the use of X-ray. Firstly, it can penetrate the imaging object easily and provide more information deep inside the object. Secondly, the background fluorescence can be avoided since X-ray was used as the excitation source to eliminate the autofluorescence, which helps to further improve the spatial resolution of optical imaging. As a hybrid X-ray/optical imaging modality, XLCT can obtain both the anatomical and the functional information simultaneously and is becoming a promising technique for fundamental research and preclinical experiments.

Continuous efforts have been made in XLCT imaging since it was first demonstrated by Xing's group [5]. The narrow-beam [10] and pencil-beam XLCT [3] showed good spatial resolution and imaging depth at the cost of long imaging time. For fast imaging, cone beam XLCT (CB-XLCT) imaging systems were investigated [1, 2, 4, 11] and experiments with simulations and phantoms demonstrate that it is more efficient and suitable for *in-vivo* research. In *in-vivo* studies, with the circulation, accumulation and metabolism of an X-ray excited nanophosphor, its concentrations in different organs or tissues may be quite different [12]. However, due to high scattering properties of biological tissues, the reconstruction of CB-XLCT is an ill-posed and ill-conditioned problem. Though some effort has been put on the differentiation of adjacent luminescence targets filled with different nanophosphors [14], there have been no studies to resolve adjacent luminescent targets with different concentrations so far.

Previous studies indicate that nanophosphors of different concentrations may have different excitation behaviors when excited by X-rays with different energy [13]. In this study, to resolve targets with different concentrations, a multi-voltage excitation scheme was first proposed. Based on the images reconstructed from, the principal component analysis (PCA) is applied to multi-voltage XLCT reconstructions to separate targets with different behaviors. Imaging experiments with physical phantoms demonstrate the feasibility of the proposed method on resolving two adjacent targets with different concentrations.

II. METHODS

A. Forward and inverse problems

X-rays emitted from the X-ray source travel through tissues or a phantom, and irradiate nanophosphors inside to emit visible or near-infrared light (NIR). The process can be expressed as follows [2]:

$$S(r)=\varepsilon X(r)\rho(r) \tag{1}$$

where $S(r)$ is the light emitted, ε is the light yield of the nanophosphors, $X(r)$ and $\rho(r)$ represent the X-ray intensity and nanophosphor concentration at position r, respectively. According to Lambert-Beers' law, the X-ray intensity distribution in the object of imaging can be expressed as:

$$X(\mathrm{r}) = X_0 \exp\{-\int_{r_0}^{r} \mu_t(\tau)\,\mathrm{d}\tau\} \tag{2}$$

where X_0 is the X-ray source intensity at the initial position r_0, and $\mu_t(\tau)$ is the X-ray attenuation coefficient of tissues at position τ, which can be obtained from the CT data.

*These authors contribute equally.

This work is partially supported by the National Natural Science Foundation of China under Grant No. 81230035

DOI: 10.12059/Fully3D.2017-11-3203031

As described previously in [1, 2], the propagation of emitted light in biological tissues can be modeled by the following diffusion equation (DE):

$$-\nabla[D(r)\nabla\Phi(r)]+\mu_a(r)\Phi(r)=S(r) \quad (3)$$

where $\Phi(r)$ is the photon fluence at position r, $D(r)$ is diffusion coefficient and can be calculated by $D(r)=(3(\mu_a(r)+\mu_s'(r)))^{-1}$, where $\mu_a(r)$ and $\mu_s'(r)$ are the absorption and reduced scattering coefficient of the tissue, respectively.

By using the finite-element method (FEM), (2) and (3) can be discretized into the following matrix equation representing the relationship between the nanophosphor concentration ρ and the photon measurement Φ_{meas}:

$$W\rho=\Phi_{\text{meas}} \quad (4)$$

where W is the weighted matrix used to map the unknown nanophosphor distribution ρ to the known measurements $\Phi_{meas.}$ In this study, for photon measurements acquired at certain X-ray tube voltage, the unknown ρ is obtained by solving (4) using the algebraic reconstruction technique (ART) with nonnegative constraints.

B. PCA method

Suppose the reconstructed multi-voltage XLCT images are denoted as $X=\{X_1, X_2, \ldots, X_i, \ldots, X_N\}$, while N is the number of X-ray voltages used in the experiment, and X_i is the reconstructed distribution of a given voltage, represented as a M column vector consisting of all pixels. In this study, to resolve targets with different concentrations, PCA is applied on reconstructed XLCT images obtained at different X-ray tube voltages. Then input data for PCA can be arranged as a $M \times N$ matrix X and its principal components can be obtained by:

$$P=X_0\times E \quad (6)$$

where X_0 is a data set obtained from X by subtracting its mean value, and E is the eigenvector matrix. The column of E is the eigenvector of the following matrix:

$$L=\frac{1}{M-1}X_0^TX_0 \quad (7)$$

The j-th column of P is the j-th principal component, PC_j, which is a linear combination of X_0. Generally, PC_1 represents approximately the mean value of two variables in X_0, and PC_2 represents difference of two variables in X_0. As described in [8, 14], the absolute values of positive and negative elements of PC_2 may reflect the positive and negative parts of the image deviated from PC_1, and therefore can be used to illustrate different distributions of nanophosphors within the imaged object.

C. Setups of phantom experiments

A custom-made CB-XLCT system developed in our laboratory was adopted to conduct the phantom experiments [1, 4]. A schematic diagram of the imaging system is shown in Fig. 1.The XLCT system consists of a micro-focus X-ray source (Source-Ray, SB-80-500, NY), a highly sensitive

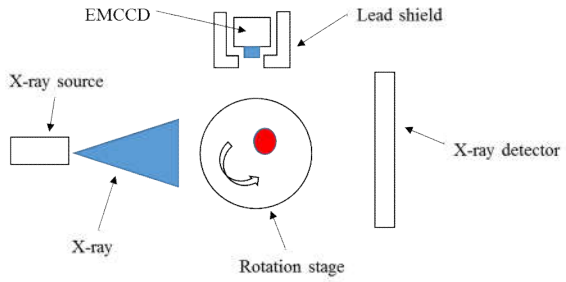

Fig. 1. Schematic diagram of the CB-XLCT system.

electron-multiplying CCD (EMCCD) camera (iXon DU-897, Andor, U.K.), which is coupled with a 50-mm f/1.8D lens (Nikon, Melville, NY), and a CMOS X-ray flat-panel detector (2923, Dexela, U.K.) for high resolution CT imaging. The X-ray source is composed of a 1.4 cm thick tungsten rectangular enclosure (5×5×11 cm), and the max voltage of the X-ray source is 80 kV and the max current is 0.5 mA. The CMOS flat-panel detector has a image matrix of 3888× 3072, with pixel size of 74.8 μm. The EMCCD camera is positioned perpendicular to the source-detector axis and collects light images of size 512×512. A lead shield with a hole of diameter 5 cm was positioned in front of the CCD camera to minimize X-ray ionizing radiation.

The configuration of the physical phantom is shown in Fig. 2. The phantom was a transparent glass cylinder with outside diameter of 3.0 cm. The cylinder was filled with 1% intralipid and water, with the absorption coefficient μ_a =0.02 cm^{-1} and reduced scattering coefficient μ_s'=10 cm^{-1}. Two small transparent glass tubes with outer diameter of 0.4 cm were positioned inside the cylinder, containing nanophosphors ($Y_2O_3:Eu^{3+}$, Jiangxi Illuma Fluorescent Materials Co., Ltd., China) with concentrations of 50 mg/ml and 100 mg/ml, respectively. The edge-to-edge distance (EED) of the two tubes was set to 0 mm, which was used to mimic two adjacent organs.

The nanophosphors in the phantom were irradiated by a series of X-ray voltages ranging from 40 kV to 80 kV under a constant current of 0.5 mA. The integration time of EMCCD was set to 0.3 s, and the EM gain was set to 260, with 1×1 binning. The projection images were acquired at a 15° step during a 360° angle span. Different combinations of X-ray excitation voltages were listed in Table 1. For CT imaging, full-angle X-ray projections were obtained with a step of 1 degree, resulting in 360 angular positions. The integrating time for each projection was 600 ms.

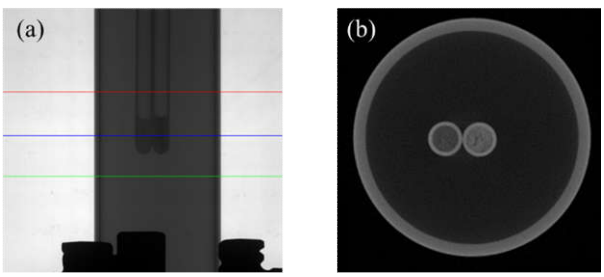

Fig. 2. Illustration of the second phantom experiment. (a) Representative X-ray projection of the phantom. The region between the red and green lines is used for this study. (b) Representative CT image slice of the phantom, corresponding to the slice indicated by the blue line in (a). The left tube contains nanophosphors of 50 mg/ml, and the right one contains 100 mg/ml, respectively.

Table 1. Different combinations of X-ray voltages used in the phantom experiments

case #	Number of X-ray voltages	X-ray voltages (kV)
case 1	5	40,50,60,70,80
case 2	4	40,50,60,70
case 3	3	40,50,60
case 4	2	40,50

For XLCT reconstruction, the reconstruction field was a 3D region of size 3.0 cm × 3.0 cm × 2.2 cm, and the phantom was discretized into 2314 nodes and 10,909 tetrahedral elements. All the reconstructions were terminated after 300 ART iterations. For cone-beam CT reconstruction, the widely-used Feldkamp-Davis–Kress (FDK) was employed.

III. RESULTS

Figure 3 shows the results of reconstructed XLCT tomographic images, which were obtained at different X-ray voltages. It indicates that it is difficult to resolve the two adjacent luminescence targets by conventional reconstruction algorithm.

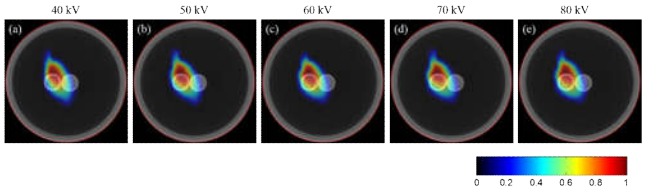

Fig. 3. Tomographic images of nanophosphor distributions in the phantom experiment reconstructed from EMCCD measurements acquired at a given voltages (40, 50, 60, 70, and 80 kV. Z=1.1 mm). The red curves in each image depict the phantom boundary.

Figure 4 shows the PC2-XLCT images generated from different voltage combinations. In cases 1 to 3, the tube with 50 mg/ml nanophosphor can be reflect by negative PC2-XLCT elements, while the tube with 100 mg/ml nanophosphors can be reflect by positive PC2-XLCT elements. However in case 4, though two tubes can be distinguished by positive and negative PC2-XLCT component, and their locations were opposite to other three case. Either the tube is reflected by the positive or negative PC2-XLCT component is determined by the calculated eigenvector matrix *E*. The results shown in Fig. 4. demonstrate that the two tubes with different concentrations of nanophosphors can be separated in all cases by the proposed PCA applied on reconstructed multi-voltage XLCT images.

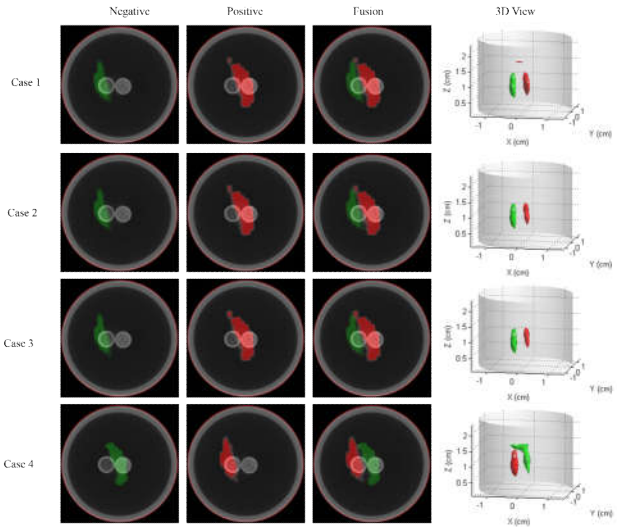

Fig. 4. Tomographic (z =1.1 cm) and 3D results of PC2 obtained from different combinations of tube voltages. All the images are displayed in the same range.

IV. CONSLUSIONS

Due to the ill-posedness and ill-condition of CB-XLCT, it is difficult to resolve adjacent luminescence targets or adjoined functional structures that are labeled with the same nanophosphors. Because nanophosphors with different concentrations have different excitation behaviors under various X-ray voltages, the problem can be resolved by a multivariate image analysis method. The feasibility of the method is demonstrated by phantom experiments with two tubes (EED=0) containing different nanophosphor concentrations of 50 and 100 mg/ml. The proposed method can be used further in *in-vivo* experiments, such as studies on the metabolism of drugs. However, the multi-voltage data acquisition increases the imaging time proportionally. More efforts should be devoted to reduce imaging time and the differentiation of more targets with different concentrations.

REFERENCES.

[1] X. Liu, Q. Liao and H. Wang, Fast X-Ray Luminescence Computed Tomography Imaging, Biomedical Engineering, IEEE Transactions on, vol. 61, pp. 1621-1627, 2014.

[2] D. Chen, S. Zhu, H. Yi, X. Zhang, D. Chen, J. Liang, and J. Tian, Cone beam X-ray luminescence computed tomography: A feasibility study, MED PHYS, vol. 40, pp. 031111, 2013.

[3] C. Li, K. Di, J. Bec, and S.R. Cherry, X-ray luminescence optical tomography imaging: experimental studies, OPT LETT, vol. 38, pp. 2339, 1 2013.

[4] X. Liu, Q. Liao and H. Wang, In vivo x-ray luminescence tomographic imaging with single-view data, OPT LETT, vol. 38, pp. 4530-4533, 2013.

[5] C.M. Carpenter, C. Sun, G. Pratx, R. Rao, and L. Xing, Hybrid X-ray/optical luminescence imaging: Characterization of experimental conditions, MED PHYS, vol. 37 , pp. 4011, 2010.

[6] A. Cong and G. Wang, A finite-element-based reconstruction method for 3D fluorescence tomography, OPT EXPRESS, vol. 13, pp. 9847-9857, 2005.

[7] H. Gao and H. Zhao, Multilevel bioluminescence tomography based on radiative transfer equation Part 2: total variation and l1 data fidelity, OPT EXPRESS, vol. 18, pp. 2894-2912, 2010.

[8] H. Pu, W. He, G. Zhang, B. Zhang, F. Liu, Y. Zhang, J. Luo, and J. Bai, Separating structures of different fluorophore concentrations by principal component analysis on multispectral excitation-resolved fluorescence tomography images, BIOMED OPT EXPRESS, vol. 4, pp. 1829, 2013.

[9] Y. Zhou, H. Guang, H. Pu, J. Zhang, and J. Luo, Unmixing multiple adjacent fluorescent targets with multispectral excited fluorescence molecular tomography, APPL OPTICS, vol. 55, pp. 4843-4849, 2016.

[10] G. Pratx, C.M. Carpenter, C. Sun, R.P. Rao, and L. Xing, Tomographic molecular imaging of X-ray-excitable nanoparticles, OPT LETT, vol. 35, pp. 3345-7, 2010.

[11] G. Zhang, F. Liu, J. Liu, J. Luo, Y. Xie, and L. Xing, Cone Beam X-ray Luminescence Computed Tomography Based on Bayesian Method, IEEE T MED IMAGING, pp. 1-1, 2016.

[12] M. Choi, K. Choi, S. Ryu, J. Lee, and C. Choi, Dynamic fluorescence imaging for multiparametric measurement of tumor vasculature, J BIOMED OPT, vol. 16, pp. 046008-046008, 2011.

[13] Y. Liu, W. Chen, S. Wang, A.G. Joly, S. Westcott, and B.K. Woo, X-ray luminescence of LaF3: Tb3+ and LaF3: Ce3+, Tb3+ water-soluble nanoparticles, J APPL PHYS, vol. 103 , pp. 063105, 2008.

[14] X. Liu, Q. Liao, H. Wang, and Z. Yan, Excitation-resolved cone-beam X-ray luminescence tomography, J BIOMED OPT, vol. 20, pp. 70501, 2015.